Modeling of Nonlinear Hysteresis in Elastomers

H.T. Banks, Gabriella A. Pinter and Laura K. Potter
Center for Research in Scientific Computation
North Carolina State University
Raleigh, NC 27695-8205 USA

M.J. Gaitens and L.C. Yanyo
Thomas Lord Research Center
Lord Corporation
Cary, NC 27511-7900 USA

Abstract

We discuss issues related to modeling of nonlinearities and hysteresis arising in a class of filled elastomers. Quasi-static and dynamic models are presented in the context of simple elongation of a filled rubber-like rod. Theoretical, computational and experimental results are given.

1 Introduction

The interest in rubber-based products has, in recent years, extended far beyond the traditional uses in tires, seals and passive damping devices. Most recently, the interest in rubber-like smart or active material devices has motivated a number of efforts on both basic and applied aspects of the scientific and engineering research required for a smart elastomer technology.

Smart material structures and fluids ([11], [23]) are generally understood to be structure and fluid composites that possess the capability to sense and actuate in a controlled manner in response to variable ambient stimuli. These are in actuality smart material systems which involve combinations of advanced sensors, actuators and microprocessors. Effective practical use of these systems in specific applications depends on fundamental developments related to a number of important modeling issues involving these composites. In particular one must have (i) models for the composite host system including sensors and actuators and (ii) models describing host system responses to input signals to the actuator. The first of these is the inactive host system model while the latter refers to the system undergoing actuation in response to stimulation. For example, detailed discussions of issues related to models for self-sensing, self-actuating structures based on piezoceramic sensors/actuators can be found in [11]. Piezoceramic-based smart systems are a rapidly maturing technological field with a large literature (a substantial number of references are given in [11]). Another class of systems based on magnetorheological (MR) solids and fluids is far less developed and questions related to these systems are the main focus of our discussions in this presentation.

MR elastomers [29],[30], which are solid analogs of MR fluids, are rubber-like composite structures filled with active as well as inactive substances. Magnetically permeable particles (such as iron) are added to a viscoelastic polymeric material prior to crosslinking. A strong external magnetic field is applied before and during crosslinking. This field induces dipole moments within the

particles, which seek minimum energy states. Particle chains with collinear dipole moments are formed and curing of the polymeric host material locks the chains in place. The resulting product is a composite material with variable elastic modulus (maximum modulus changes of between 30% and 40% have been reported in experimental data [29] in response to an applied external magnetic field).

Models of the response of the elastomer to an applied magnetic field involve induced stress as a function of induced magnetic flux density. This in turn involves understanding the dependence of the elastic modulus on the induced magnetic flux. Modeling, which is truly in its infancy, can be based on magnetic dipole interactions between adjacent particles. Since the value of the magnetic permeability varies dramatically between particles and host material, it is to be expected that homogenization techniques [12], [18], [25] will play a significant role in any careful modeling of effective moduli. Early results [40] suggest that the magnetic permeability is a nonlinear function of the magnetic potential and hence nonlinear homogenization [17] formulations will be necessary to develop models in category (ii) above.

Our discussions here will be on models for the dynamical response of the composite host, i.e., *inactive* filled elastomers or filled viscoelastic structures. Thus we focus on issues related to requirement (i) above. Such models involve nonlinear and hysteretic formulations in a significant way. We describe some of our efforts with model development, estimation and experimental verification. In addition to providing basic understanding of filled rubber responses to loads, these efforts are a necessary first step in the development of a smart elastomers technology.

2 Nonlinear models for extension

Our early efforts focused on understanding the nonlinearities inherent in the dynamic response of filled rubber-like compounds to applied loads and impulsive disturbances. First we outline the development of our basic model, which is based on neo-Hookean principles. Comparison of this model with experimental data motivated the need for a more general model, which we will describe in Section 2.2.

2.1 A neo-Hookean model

Most models for elastomers found in the literature are based on strain energy function (SEF) and finite strain theories (see [6], [26], [36], [15] and the references therein). Together with momentum balance laws, the SEF and finite strain theories can be used to derive dynamic equations of motion. To illustrate our approach here, we take a simple example: an isotropic, incompressible, rubber-like rod with a tip mass undergoing simple elongation with a finite applied stress in the principle axis direction $x_1 = x$. A detailed development can be found in [6].

For neo-Hookean materials the finite stress theory (or the Mooney theory with SEF $U = C_1(I_1 - 3)$) leads to a true stress $T = \frac{E}{3}(\lambda_1^2 - \frac{1}{\lambda_1})$, or an engineering stress

$$S = \frac{T}{\lambda_1} = \frac{E}{3}(\lambda_1 - \frac{1}{\lambda_1^2}).$$

Here λ_i are the principle extension ratios, which represent the deformed length of unit vectors parallel to the principal axes (the axes of zero shear stress), and the first strain invariant I_1 is

$I_1 = \lambda_1^2 + \lambda_2^2 + \lambda_3^2$. In this case the dynamical problem reduces to a one-dimensional problem. In terms of the finite strain $\tilde{e}_{xx}$ and the deformation u in the x direction we have

$$\lambda_1^2 = 1 + 2\tilde{e}_{xx} = 1 + 2\frac{\partial u}{\partial x} + \left(\frac{\partial u}{\partial x}\right)^2 = \left(1 + \frac{\partial u}{\partial x}\right)^2.$$

This can be used in the Timoshenko theory for longitudinal vibrations of a rubber bar with a tip mass to obtain

$$\begin{aligned} &\rho A_c \frac{\partial^2 u}{\partial t^2} - \frac{\partial S}{\partial x} = 0 \qquad 0 < x < \ell \\ &M\frac{\partial^2 u}{\partial t^2}(t,\ell) = -S|_{x=\ell} \ + F(t) + Mg \end{aligned} \tag{2.1}$$

where ρ is the mass density, $F(t)$ is the applied external force, A_c is the cross sectional area, M is the tip mass, g is the gravitational constant, and the internal stress resultant S is given by

$$S = \frac{A_c E}{3}(\lambda_1 - \frac{1}{\lambda_1^2}) + C_D A_c \frac{\partial \lambda_1}{\partial t} = \frac{A_c E}{3}\tilde{g}\left(\frac{\partial u}{\partial x}\right) + C_D A_c \frac{\partial^2 u}{\partial t \partial x}.$$

Here E is the generalized modulus of elasticity and $\tilde{g}(\xi) = 1 + \xi - (1+\xi)^{-2}$. A Kelvin-Voigt damping term with coefficient C_D is included in the stress as a first attempt to model damping. This leads to the nonlinear partial differential equation

$$\rho A_c \frac{\partial^2 u}{\partial t^2} - \frac{\partial}{\partial x}\left(\frac{EA_c}{3}\tilde{g}(\frac{\partial u}{\partial x}) + A_c C_D \frac{\partial^2 u}{\partial t \partial x}\right) = 0 \qquad 0 < x < \ell \tag{2.2}$$

$$M\frac{\partial^2 u}{\partial t^2}(t,\ell) = -\left(\frac{EA_c}{3}\tilde{g}(\frac{\partial u}{\partial x}) + A_c C_D \frac{\partial^2 u}{\partial t \partial x}\right)|_{x=\ell} + F(t) + Mg \tag{2.3}$$

$$u(t,0) = 0 \tag{2.4}$$

$$u(0,x) = \Delta(x), \quad u_t(0,x) = 0, \tag{2.5}$$

for dynamic longitudinal displacements of a neo-Hookean material in extension. The initial configuration $u(0,x)$ is given by $\Delta(x)$, with zero initial velocity.

Several theoretical and practical questions arise in connection with this model. The most fundamental is the well-posedness of the initial boundary value problem associated with (2.2)-(2.5). It is shown in [4] that a unique weak solution of (2.2)-(2.5) exists even under more general circumstances, i.e., for a broad class of nonlinearities $\tilde{g}$. This is important, since comparison between experimental data and preliminary numerical calculations outlined in [6] suggested that the neo-Hookean nonlinearity $\tilde{g}(\xi) = 1 + \xi - (1+\xi)^{-2}$ is not adequate to describe the behavior of filled elastomers. By allowing for a more general form for the nonlinear function $\tilde{g}$, we can refine the model using inverse problem techniques.

2.2 A general nonlinear constitutive law

To better capture the dynamic behavior of elastomers in extension, a general nonlinear function $\tilde{g}$ can be used in (2.2)-(2.5) in place of the neo-Hookean form. Using parameter estimation techniques,

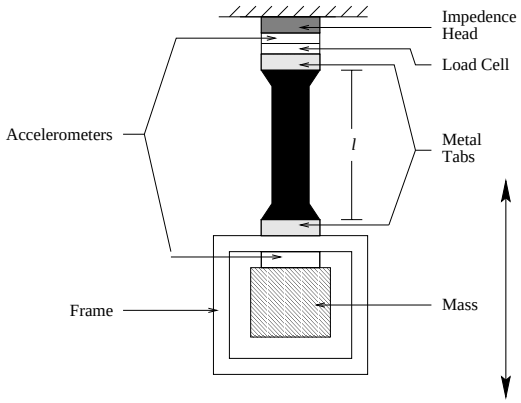

Figure 1: Rod with tip mass under tension.

an appropriate form for $\tilde{g}$ and the unknown constants ρ, E and C_D can be determined. Preliminary work in the quasi-static regime detailed in [6] provided an encouraging first step in estimating $\tilde{g}$, and gave us insight in formulating an inverse problem for the full dynamic model (2.2)-(2.5). With this in mind, we designed a series of dynamic experiments that were performed at Lord Corporation.

Our initial experiments included dynamic free release and impulse response tests with cylindrical elastomeric samples in extension. The elastomer was suspended vertically with the top end ($x = 0$) fixed, and a frame was attached to the lower end (see Figure 1). Varying amounts of extra mass were attached to this frame, which also served to house an accelerometer. Another accelerometer, placed at the top of the sample, was used to verify the clamped boundary condition at the fixed end.

For the free release experiment, the rubber rod was lifted together with the frame and the tip mass so that no compression or extension occurred. Then the support was removed, allowing the mass to fall freely. This type of experiment was repeated with unfilled and lightly filled carbon black samples, while a similar experiment was done with a highly filled sample with a 9.29 lb tip mass.

The force data collected by the load cell on top of the sample were used in estimating the unknown parameters $q = \{g, \rho, E, C_D\}$ in (2.2)-(2.5) by minimizing

$$J(q) = \frac{1}{2}\sum_{i=1}^{N} |z_i - A_c\sigma(\frac{\partial u}{\partial x}(t_i, 0; q))|^2$$

over q in some admissible parameter space Q. Here z_i, $i = 1, \ldots, M$ represent the experimental observations of the force at the fixed end, and u is the solution of (2.2)-(2.5) corresponding to the parameters q. Initially we solved this inverse problem using observations z_i from the unfilled natural rubber.

Based on our previous work with the quasi-static case (see [6]), we tested two forms for the function $\tilde{g}$ in the inverse problem. First $\tilde{g}$ was chosen as the best possible linear function, followed by choosing the best $\tilde{g}$ from a class of four-term piecewise linear splines. Figure 2 depicts the best fit to the data that can be achieved using a linear $\tilde{g}$, and definitely suggests that a nonlinear function is required to successfully model the behavior of the elastomer. Figure 3 depicts the fit achieved using a four-term piecewise linear $\tilde{g}$. This fit is much better and captures the nonlinear behavior

as well. However, as the same experiments and calculations were repeated for lightly filled and highly filled elastomer rods, the best attainable fit deteriorated. This strongly suggested that in these cases some of the observed hysteretic behavior, which is described in detail in Section 3.3.1, also must be taken into account.

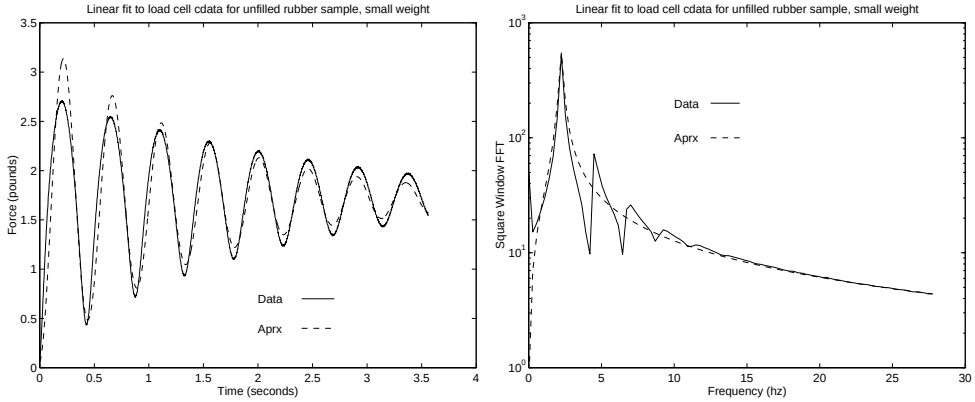

Figure 2: (left) Time domain approximation with a linear $\tilde{g}$, and (right) the FFT of the solution and the data.

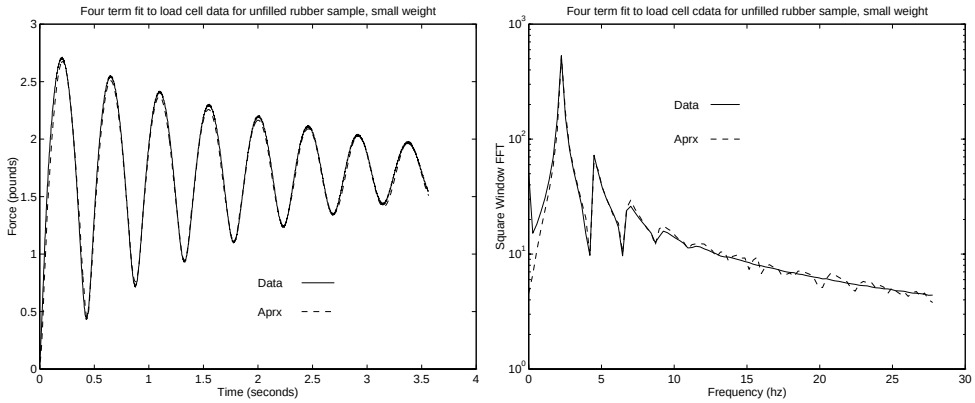

Figure 3: (left) Time domain approximation with a four-term piecewise linear $\tilde{g}$, and (right) the FFT of the solution and the data.

3 Hysteretic Models

3.1 Conceptual Issues

The efforts described above on nonlinear aspects of rubber dynamics combined with quasi-static experimental observations outlined in 3.3.1 conclusively demonstrated the importance of hysteresis in our understanding of filled host dynamic response. This is an often-studied and seldom resolved aspect of viscoelastic material dynamics which usually begins with constitutive stress-strain formulations. A huge literature on modeling of viscoelastics and rubbers currently exists (e.g., see [13], [14], [16], [21], [39], among the many discussed in [43]). Two types of modeling approaches

for stress-strain relationships can be found in the literature on viscoelastic materials. One is developed on the basis of the phenomenological mechanical behavior of the samples, while the other concentrates on the microscopic behavior of the particles and fibers, such as the changes in the crosslinking and the contour length of fibers, and on the different relaxation times of fibers. The most fundamental model is the Boltzmann integral model, which attempts to capture the viscosity of the material and the history dependence of the stress on the strain and/or strain rate; the latter characteristic is a signature of rubber materials. As is well known, the Boltzmann integral can be reduced easily to some familiar differential models, e.g., Kelvin-Voigt and Maxwell. Due to the fundamental importance of the Boltzmann integral, we digress here to briefly outline its foundation.

The major assumption (a principle of superposition) made by Boltzmann is that linear models can be added together to generate more complicated models (see [31]). This assumption is referred to as the Boltzmann Superposition Principle (see [20], p. 6).

One can generalize the basic Kelvin-Voigt and Maxwell models (see [43], Chap. 3 for a detailed discussion) to relate the stress and strain by

$$\varepsilon(t) = \sigma_0 J(t) H(t) \quad \text{where} \quad \sigma = \sigma_0 H(t) \tag{3.6}$$

$$\sigma(t) = \varepsilon_0 Y(t) H(t) \quad \text{where} \quad \varepsilon = \varepsilon_0 H(t) \tag{3.7}$$

for functions $J(t)$ and $Y(t)$ that are termed the creep compliance function and the relaxation modulus function, respectively. Here H is the usual Heaviside function. Boltzmann generalized the above models to account for variables $\sigma(t)$ and $\varepsilon(t)$ (e.g., the results from stretch and relaxation tests) by considering a succession of infinitesimal steps $d\varepsilon(t)$ for (3.6) or a succession of infinitesimal steps $d\sigma(t)$ for (3.7).

As a result, one obtains

$$d\sigma(t) = d\varepsilon(s) Y(t-s) H(t-s) \ . \tag{3.8}$$

One can rewrite $d\varepsilon(s) = \frac{d\varepsilon(s)}{ds} ds$, set $t \geq s$, and integrate (3.8) from $-\infty$ to t to obtain

$$\sigma(t) = \int_{-\infty}^{t} Y(t-s) \frac{d\varepsilon(s)}{ds} ds \ .$$

A similar expression for ε in terms of the kernel J and the history of the stress rate can be obtained. The above integral is referred to as a Boltzmann integral since it conforms with the fundamentals of superposition as enunciated by Boltzmann. Physical models that consist of a continuum of springs and dashpots are often associated with such integrals since they result from the limit of summing an infinite number of Maxwell and Kelvin-Voigt models (see [20], [43]).

Typical nonlinear behaviors of the stress and strain in rubber materials under finite (i.e., non-infinitesimal) deformation include a continuous increase of strain at decreasing rates upon loading, variable magnitudes of the strain subject to rates of loading, and different loading and unloading paths due to hysteretic memory effects. In addition, there are other nonlinear features that are particular to the samples under study. These traits can be modeled accurately to some degree using theories originated by Rivlin for finite deformations alone (e.g., see [38], [42]); however, to fully describe nonlinear viscoelastic materials, it is desirable to also consider internal chemical and physical interactions involving long chain molecules and fillers. We refer the reader to [26] for an example of derivations of internal variable models and internal solid models, which are based on the molecular point of view. The previously mentioned Kelvin-Voigt model, Maxwell model and Boltzmann integral formulation can be modified to include finite deformations by making material

the coefficients functions of $\varepsilon(t)$ and t, or by defining new laws between $\sigma(t)$ and $\varepsilon(t)$ (or more precisely, the finite strain $\tilde{e}(t)$ in the case of finite deformations). There are a number of models that involve attempts to model nonlinearity in viscoelastic material through finite deformation theories (see [20], [26], [37]). For more complete discussions we refer readers to Chapter 3 of [43] and a lengthy list of references found there.

Many of the various models in the literature have been verified qualitatively and/or numerically for specific samples under individual tests. However, due to the complex dependence of rubber composites on many physical parameters, it has been very difficult to obtain a general formulation that is reasonably simple quantitatively and that captures viscoelastic behavior across a wide range of materials. For our investigations reported on here, we have used a Boltzmann law with a nonlinear strain functional. Before turning to a summary of our findings to date, we briefly discuss the often controversial subject of pseudo-phenomenological models versus physics-based or internal models in viscoelasticity.

As we have already noted, among the most often used formulations to account for hysteresis is the Boltzmann superposition model (also called the Maxwell solid in history integral form) which is based on the hypothesis that the stress is strain rate dependent through a convolution relationship [16]

$$\sigma(t) = C\varepsilon(t) + \int_{-\infty}^{t} k(t-\tau)\dot{\varepsilon}(\tau)\, d\tau\,. \tag{3.9}$$

For many materials, this linear relationship is inadequate to capture the behavior and internal characteristics manifested in experiments and one must turn to nonlinear generalizations of the form

$$\sigma(t) = f_e(\varepsilon(t)) + \int_{-\infty}^{t} k(t-\tau) f_v(\dot{\varepsilon}(\tau))\, d\tau \tag{3.10}$$

or

$$\sigma(t) = f_e(\varepsilon(t)) + \int_{-\infty}^{t} k(t-\tau)\frac{d}{d\tau} f_v(\varepsilon(\tau))\, d\tau\,. \tag{3.11}$$

The nonlinearities f_e and f_v are often associated with the material's elastic and viscoelastic properties, respectively. Even if one or both are assumed linear, they must be identified along with the kernel k from experimental data. If this is done with little or no mechanistic assumptions that place constraints on the form of f_e, f_v, k (e.g., see [1],[2],[3] and references therein), such an approach renders the Boltzmann modeling a phenomenological approach. If, on the other hand, one uses physical considerations (such as in [10]) to constrain the choices of f_e, f_v, k in the inverse problem or parameter estimation procedures, the modeling attempt can be thought of as pseudo-phenomenological. In fact, it is equivalent to identifying the impulse response function and nonlinearities for certain types of (possibly physically-based) internal variable models (Maxwell solids in differential form). For example, if one considers internal strain models as in [27], [32], [33], then the basic assumption is that one has a finite number of internal "strain" variables $\varepsilon_j(t),\ j = 1, \cdots, N$, along with the strain $\varepsilon(t)$, and the stress is given by

$$\sigma(t) = f_e(\varepsilon(t)) + \sum_{j=1}^{N} c_j \varepsilon_j(t)\,. \tag{3.12}$$

The internal strains might be given by dynamics

$$\frac{d\varepsilon_j}{dt} + \frac{\varepsilon_j}{\tau_j} = f_j(\dot{\varepsilon}(t))\ ,\ j = 1, \cdots, N\,, \tag{3.13}$$

or

$$\frac{d\varepsilon_j}{dt} + \frac{\varepsilon_j}{\tau_j} = \frac{d}{dt} f_j(\varepsilon(t)) = f_j'(\varepsilon(t))\dot{\varepsilon}(t) \ , \ j = 1, \cdots, N \, . \tag{3.14}$$

If we write the solutions of the equations by

$$\varepsilon_j(t) = \int_{-\infty}^{t} e^{-(t-\tau)/\tau_j} f_j(\dot{\varepsilon}(\tau)) \, d\tau \tag{3.15}$$

or

$$\varepsilon_j(t) = \int_{-\infty}^{t} e^{-(t-\tau)/\tau_j} \frac{d}{d\tau} f_j(\varepsilon(\tau)) \, d\tau \, , \tag{3.16}$$

then (3.12) is completely equivalent to (3.10) or (3.11) where

$$k(t-\tau) f_v(\dot{\varepsilon}(\tau)) = \sum_{j=1}^{N} c_j e^{-(t-\tau)/\tau_j} f_j(\dot{\varepsilon}(\tau)) \tag{3.17}$$

or

$$k(t-\tau) \frac{d}{d\tau} f_v(\varepsilon(\tau)) = \sum_{j=1}^{N} c_j e^{-(t-\tau)/\tau_j} \frac{d}{d\tau} f_j(\varepsilon(\tau)) \, , \tag{3.18}$$

respectively. In this case, the Boltzmann approach under the assumptions (3.17) or (3.18) is completely equivalent to the internal variable approach. The only real difference in these two approaches lies in the implementation; i.e., one might start with (3.10) or (3.11) and attempt to identify the overall impulse response function $k(t)$ without any consideration of internal dynamics, or one might use (3.12) with (3.13) or (3.14) and attempt to identify the individual decay constants τ_j along with the coefficients c_j and nonlinearities f_j.

If, however, one assumes nonlinear internal dynamics of the form

$$\frac{d\varepsilon_j}{dt} + g_j(\varepsilon_j) = f_j(\dot{\varepsilon_j}) \ , \ j = 1, \cdots, N, \tag{3.19}$$

in place of (3.13), then (3.12) cannot be rewritten in Boltzmann form and the internal variable approach is distinct from a general Boltzmann approach. In this case, one must solve a coupled system (the overall dynamical PDE in which σ appears plus the system (3.19) coupled with (3.12)) as opposed to an implicit internal dynamics system involving (3.10) or (3.11) in the PDE's of deformation.

One might also generalize the internal variable/Boltzmann linear models by defining a generalized stress $\overline{\sigma} = (\sigma, \dot{\sigma}, \cdots, \sigma^{(n_1)})$ and generalized strain $\overline{\varepsilon} = (\varepsilon, \dot{\varepsilon}, \cdots, \varepsilon^{(n_2)})$ with internal vector dynamics

$$\frac{d\overline{\sigma}}{dt} = A\overline{\sigma} + \overline{\mathcal{F}}(\overline{\varepsilon}) \tag{3.20}$$

so that

$$\overline{\sigma}(t) = \int_{-\infty}^{t} e^{A(t-\tau)} \overline{\mathcal{F}}(\overline{\varepsilon}(\tau)) \, d\tau \, .$$

If one defines $X(t) = e^{At}$, this becomes

$$\sigma(t) = \int_{-\infty}^{t} \sum_{j=1}^{n_1} X_{1j}(t-\tau) \overline{\mathcal{F}}_j(\varepsilon(\tau), \dot{\varepsilon}(\tau), \cdots, \varepsilon^{(n_2)}(\tau)) \, d\tau, \tag{3.21}$$

which again is recognized as a generalized Boltzmann formulation. In particular, (3.11) is a special case of this formulation with $n_1 = 1$ since

$$\frac{d}{d\tau} f_v(\varepsilon(\tau)) = f_v'(\varepsilon(\tau))\dot{\varepsilon}(\tau) = \mathcal{F}(\varepsilon(\tau), \dot{\varepsilon}(\tau))\,. \tag{3.22}$$

The internal strain models of (3.12) and (3.13) can also be put in this more general form by taking $\tilde{\varepsilon} = (\varepsilon_1, \varepsilon_2, \cdots, \varepsilon_N)$ and

$$\frac{d\tilde{\varepsilon}}{dt} = A\tilde{\varepsilon} + \mathcal{F}(\dot{\varepsilon}(t))$$

so that

$$\tilde{\varepsilon}(t) = \int_{-\infty}^{t} e^{A(t-\tau)} \mathcal{F}(\dot{\varepsilon}(\tau))\, d\tau$$

and

$$\sigma(t) = f_e(\varepsilon(t)) + \overline{c} \cdot \tilde{\varepsilon}(t) = f_e(\varepsilon(t)) + \int_{-\infty}^{t} \overline{c} \cdot \left[e^{A(t-\tau)} \mathcal{F}(\dot{\varepsilon}(\tau)) \right] d\tau \tag{3.23}$$

for $\overline{c} = (c_1, c_2, \cdots, c_N)$. These considerations clearly reveal that (3.12) and (3.13) are special cases of a generalized Boltzmann approach, and the primary difference between a Boltzmann and linear internal variables approach is mainly philosophical. That is, in the Boltzmann approach, one attempts to identify the impulse response e^{At} as opposed to the internal variables approach where one is concerned with the operator A. In both situations, one must also identify the nonlinearities f_e and f_v (or $\mathcal{F}$ in (3.23)).

There is another pseudo-phenomenological approach to hysteresis found in the engineering literature on viscoelasticity that is related to our remarks above. The so-called Golla-Hughes-McTavish (or GHM) method (see [22], [24], [34] for readable summaries) can be interpreted as a nonphysics-based internal variable model approach to viscoelasticity. In this approach, one introduces additional coordinates (i.e., internal variables) in state space models to account for hysteretic behavior. The general approach uses complex modulus or loss factor data (modulus or frequency data) to fit rational polynomials representing the Laplace transform of hysteresis stress-strain relationships. Specifically, the viscoelastic hysteresis is approximated by adjoining a state variable z with frequency domain representation

$$h(s) = \frac{\alpha s^2 + \beta s}{s^2 + bs + c}\,.$$

This is equivalent to an internal dynamics of the form $\ddot{\sigma}_{ve} + b\dot{\sigma}_{ve} + c\sigma_{ve} = \alpha\ddot{\varepsilon} + \beta\dot{\varepsilon}$, or, in frequency domain, $\hat{\sigma}_{ve}\{s^2 + bs + c\} = \{\alpha s^2 + \beta s\}\hat{\varepsilon}$. This, of course, can be recognized as a special case of (3.20) by defining $\overline{\sigma} = (\sigma_{ve}, \dot{\sigma}_{ve})$, $\overline{\varepsilon} = (\varepsilon, \dot{\varepsilon}, \ddot{\varepsilon})$ and

$$\dot{\overline{\sigma}} = K\overline{\sigma} + E\overline{\varepsilon} \tag{3.24}$$

with

$$K = \begin{bmatrix} 0 & 1 \\ c & b \end{bmatrix} \quad , \quad E = \begin{bmatrix} 0 & 0 & 0 \\ 0 & \beta & \alpha \end{bmatrix}\,.$$

In the usual engineering practice, one attempts to identify c, b, α, β using frequency domain data and then adjoins this to the time domain (e.g., finite element or modal) model via (3.24). Once again, the philosophy of this approach is to identify the operator A (i.e., K) in (3.20) instead of identifying e^{At}.

The internal variable approach outlined above can be carried out for particular structures and materials by hypothesizing physics-based internal dynamics. One such example involves finite strain internal stretch variable models for viscoelastic rubbers as developed in [19] and [28]. These involve stick-slip models for the viscoelastic response to a large step-strain (see [19] and [28] for details).

3.2 Theoretical Issues

To outline our efforts to date in incorporating hysteresis in our models, we return to the example involving simple extension in a rod of cross-sectional area A_c, length ℓ, and mass density ρ, with applied force $f(t)$ at the end $x = \ell$. We assume a Boltzmann-type stress-strain law of the form

$$\sigma(t) = g_e(\varepsilon(t)) + \int_{-\infty}^{t} Y(t-s)\frac{d}{ds}g_v(\varepsilon(s), \dot{\varepsilon}(s))ds, \tag{3.25}$$

where Y is the memory kernel, and g_e and g_v are nonlinear functions accounting for the elastic and viscoelastic nonlinear responses (respectively) of the elastomer. This stress-strain law implies that the stress depends not only on the current strain but also on the history of the strain and the strain-rate.

The inclusion of both elastic and viscoelastic response functions resulted from both experimental observations and earlier work (e.g., see [26], [28]). *Elastic* materials undergoing finite deformations require the use of a nonlinear constitutive law, as discussed in Ogden [36]. This leads to the conclusion that *viscoelastic* materials would also have a nonlinear stress-strain relationship, especially in the finite deformation regime. Moreover, filled rubber exhibits hysteretic properties, which suggests the use of an integral term and the viscoelastic response function inside the integral.

As we have already noted, models for filled elastomers in extension are motivated by formulations for large deformation tensile dynamics. When properly modeled, these dynamics require *finite* strains [36], [38]

$$\tilde{e} = \frac{\partial u}{\partial x} + \frac{1}{2}\left(\frac{\partial u}{\partial x}\right)^2 = \varepsilon + \frac{1}{2}\varepsilon^2 \tag{3.26}$$

in constitutive laws, where $\varepsilon = \frac{\partial u}{\partial x}$ is the usual *infinitesimal* strain of linear elasticity (see [5] for basic modeling techniques as well as specific examples related to longitudinal (tensile) deformation models). As outlined in Section 2 above, computational and experimental results (see [6]) have confirmed that *nonlinear* constitutive laws

$$\sigma(t) = \tilde{G}_e(\tilde{e}(t)) \tag{3.27}$$

are required to model even the small deformation elastic dynamics for lightly filled elastomers. However, for more highly filled elastomers (the primary focus for both passive and active damping devices), hysteresis is present and viscoelastic behavior must be combined with basic nonlinear elastic behavior in constitutive laws of the form

$$\sigma(t) = \tilde{G}_e(\tilde{e}(t)) + \tilde{G}_v(\tilde{e}(t+s) : -\infty < s \leq 0). \tag{3.28}$$

In light of (3.26), this is equivalent to attempting to determine nonlinear maps g_e, g_v so that the constitutive law is given by

$$\sigma(t) = g_e(\varepsilon(t)) + g_v(\varepsilon(t+s) : -\infty < s \leq 0). \tag{3.29}$$

That is, modeling the nonlinear behavior between the stress and the *finite* strains $\tilde{e}$ (which are themselves nonlinear functions of the infinitesimal strains ε) can be equivalently formulated in terms of nonlinear relationships between the stress and the *infinitesimal* strains ε. Hence we equivalently assume (3.25) instead of a similar law involving the finite strains $\tilde{e}$.

We also recall that the stress-strain law (3.25) contains various standard *internal strain* or *internal variable* formulations as special cases. The ADF models of Lesieutre [32], [33] for composite materials exhibiting both elastic and anelastic displacement fields are formulated on the assumption that the host elastic material contains anelastic materials with internal strains ε_1 which are elastic strain driven. That is, the constitutive laws have the form

$$\sigma(t) = E_1\varepsilon(t) - E_2\varepsilon_1(t), \tag{3.30}$$

where the internal strain is given by

$$\begin{aligned} &\dot{\varepsilon}_1(t) + c_1\varepsilon_1(t) = c_2\varepsilon(t) \\ &\varepsilon_1(0) = 0, \end{aligned} \tag{3.31}$$

or equivalently,

$$\varepsilon_1(t) = \int_0^t c_2 e^{-c_1(t-s)}\varepsilon(s)ds.$$

Several generalizations of this formulation exist, e.g., Johnson et.al. [26], suggest that the internal strain is strain *rate* driven, i.e.,

$$\dot{\varepsilon}_1(t) + c_1\varepsilon_1(t) = c_2\dot{\varepsilon}(t). \tag{3.32}$$

Our Boltzmann-type law (3.25) (under appropriate assumptions on the past memory from $-\infty$ to 0) corresponds to an internal strain model of the form:

$$\begin{aligned} &\dot{\varepsilon}_1(t) + c_1\varepsilon_1(t) = \frac{d}{dt}g_v(\varepsilon(t), \dot{\varepsilon}(t)) \\ &\varepsilon_1(0) = 0. \end{aligned} \tag{3.33}$$

This form was chosen after we found that neither (3.30) nor (3.32) provided laws that could describe our data.

Experimental observations of the quasi-static behavior of elastomers (see Section 3.3.1) indicate that these materials possess different nonlinear viscoelastic responses in loading ($\dot{\varepsilon} > 0$) and unloading ($\dot{\varepsilon} < 0$). This led to our choice of a piecewise continuous form for the viscoelastic response function g_v:

$$g_v(\varepsilon(s), \dot{\varepsilon}(s)) \quad = \quad \begin{cases} g_{vi}(\varepsilon(s)) & \dot{\varepsilon}(s) > 0 \\ g_{vd}(\varepsilon(s)) & \dot{\varepsilon}(s) < 0. \end{cases} \tag{3.34}$$

Here we require g_{vi} and g_{vd} to be continuous (and generally nonlinear) functions. This difference between loading and unloading is more pronounced as the amount of filler increases in the material. We define the points t_i, $i = 1, \ldots, K$ as the "turning points," or the points in time for which $\dot{\varepsilon} = 0$. The function g_v need not be continuous at the turning points, so we must interpret the derivatives

in (3.25),(3.33) as distributional derivatives. That is, delta functions are involved in differentiating the composite functions $g_v(\varepsilon, \dot{\varepsilon})$, or equivalently, integration by parts is valid.

Earlier calculations and experiments suggested that the rubber does not exhibit infinite memory, but significantly depends only on a history of finite length r. That is, the memory kernel Y is such that $Y(\xi) \approx 0$ for $\xi \geq r$. Therefore we can approximate (3.25) by

$$\sigma(t) = g_e(\varepsilon(t)) + \int_{t-r}^{t} Y(t-s) \frac{d}{ds} g_v(\varepsilon(s), \dot{\varepsilon}(s)) ds. \tag{3.35}$$

Integrating by parts in (3.35) and assuming $t_K < t < t_{K+1}$, we have

$$\begin{aligned} \sigma(t) &= g_e(\varepsilon(t)) + \int_{t-r}^{t} \dot{Y}(t-s) g_v(\varepsilon(s), \dot{\varepsilon}(s)) ds + Y(0) g_v(\varepsilon(t), \dot{\varepsilon}(t)) \\ &+ \sum_{k=1}^{K} Y(t-t_k)(-1)^{k+1} [g_{vi}(\varepsilon(t_k)) - g_{vd}(\varepsilon(t_k))], \end{aligned} \tag{3.36}$$

where we have used $Y(r) \approx 0$. This is precisely the form of the stress-strain law that we used in the calculations reported on below.

To develop the corresponding dynamic model for simple extension, we must incorporate these jump terms into our formulation. Let $u(t,x)$ denote the displacement at time t of the section of the rod originally located at x, $0 \leq x \leq \ell$. If we assume that the rod begins its motion at rest with possible deformation $\Delta(x)$ and fixed end at $x = 0$, we obtain

$$\begin{aligned} \rho A_c \frac{\partial^2 u}{\partial t^2} = \frac{\partial}{\partial x} \Bigg[& A_c \tilde{g}_e(\frac{\partial u}{\partial x}) + A_c Y(0) g_v(\frac{\partial u}{\partial x}, \frac{\partial^2 u}{\partial x \partial t}) + A_c \int_{t-r}^{t} \dot{Y}(t-s) g_v(\frac{\partial u}{\partial x}, \frac{\partial^2 u}{\partial x \partial t}) ds \\ & + A_c \sum_{k=1}^{K} Y(t-t_k)(-1)^{k+1} [g_{vi}(\frac{\partial u}{\partial x}(t_k)) - g_{vd}(\frac{\partial u}{\partial x}(t_k))] \Bigg] \quad \text{for} \quad 0 < x < \ell \end{aligned} \tag{3.37}$$

$$\begin{aligned} A_c \Bigg[& g_e(\frac{\partial u}{\partial x}(t)) + Y(0) g_v(\frac{\partial u}{\partial x}(t), \frac{\partial^2 u}{\partial x \partial t}(t)) + \int_{t-r}^{t} \dot{Y}(t-s) g_v(\frac{\partial u}{\partial x}(s), \frac{\partial^2 u}{\partial x \partial t}(s)) ds \\ & + \sum_{k=1}^{K} Y(t-t_k)(-1)^{k+1} [g_{vi}(\frac{\partial u}{\partial x}(t_k)) - g_{vd}(\frac{\partial u}{\partial x}(t_k))] \Bigg] \Bigg|_{x=\ell} = f(t) \end{aligned} \tag{3.38}$$

$$u(t,0) = 0 \tag{3.39}$$

$$u(0,x) = \varphi_0 \tag{3.40}$$

$$u_t(0,x) = 0 \tag{3.41}$$

$$u(t,x) = \varphi_1, \quad t < 0. \tag{3.42}$$

We may also include an (internal) Kelvin-Voigt damping term $C_D u_{xxt}$ ($C_D > 0$) in the model. In general the resulting model should be written in variational form

$$\rho A_c \ddot{u} - C_D u_{xxt} - \frac{\partial}{\partial x}\left(A_c g_e(\frac{\partial u}{\partial x}) + A_c Y(0) g_v(\frac{\partial u}{\partial x}, \frac{\partial^2 u}{\partial x \partial t}) + A_c \int_{t-r}^{t} \dot{Y}(t-s) g_v(\frac{\partial u}{\partial x}(s), \frac{\partial^2 u}{\partial t \partial x}(s)) ds \right.$$

$$\left. + A_c \sum_{k=1}^{K} Y(t-t_k)(-1)^{k+1}[g_{vi}(\frac{\partial u}{\partial x}(t_k)) - g_{vd}(\frac{\partial u}{\partial x}(t_k))] \right) = F(t) \quad \text{in } V^* \tag{3.43}$$

$$u(t,0) = 0 \tag{3.44}$$

$$u(0,x) = \varphi_0 \tag{3.45}$$

$$u_t(0,x) = 0 \tag{3.46}$$

$$u(t,x) = \varphi_1, \quad t < 0. \tag{3.47}$$

for an appropriately chosen Hilbert space V. This presumes, of course, that we have sufficient smoothness so that evaluation of $\frac{\partial u}{\partial x}$ at t_i makes sense and $\frac{\partial}{\partial x}(g_{vi}(\frac{\partial u}{\partial x}(t_i))), \frac{\partial}{\partial x}(g_{vd}(\frac{\partial u}{\partial x}(t_i))) \in V^*$. For this particular example, one takes $V = H_L^1(0,\ell) = \{\phi \in L^2(0,\ell) | \phi' \in L^2(0,\ell), \phi(0) = 0\}$. The important question of well-posedness of the system (3.43)-(3.47) is treated carefully in [9]. We have shown that under certain assumptions there exists a unique weak solution of the system (3.43)-(3.47). Specific definitions and results are quite technical in nature and we refer the interested reader to [9].

3.3 Experimental and computational results

With the aid of inverse problem techniques and experimental data, we may address the validity of the quasi-static model (3.25) and the dynamic model (3.37)-(3.42) for filled elastomers. We designed and implemented both quasi-static and dynamic experiments for elastomers in tension, and used the data we gathered to estimate parameters associated with our models.

Since the quasi-static case is simpler to study experimentally and computationally, we first investigated the inverse problem for the constitutive model (3.25). Using the knowledge gained from the quasi-static case, we then returned to the full dynamic case and solved the inverse problem associated with the model (3.37)-(3.42).

3.3.1 Quasi-static inverse problems

In a series of experiments at Lord Corporation, we tested the quasi-static behavior of filled rubber rods in simple uniaxial tension. Cylindrical rubber samples were manufactured with metal flanges on each end and secured vertically into an Instron 4204 machine. The bottom end of the sample was secured so that it would remain fixed, while the upper end was attached to a load cell and a horizontal crossbar, as in Figure 4. The samples used in this experiment were a silica-filled silicone elastomer and three carbon black-filled natural rubbers, including lightly filled, medium filled and highly filled samples.

Using the software package STD4200, a sequence of displacements $\Delta(t)$ was programmed into the machine and the resulting loading forces $f(t)$ were recorded. The load and displacement data was then converted into the infinitesimal strain $\varepsilon(t)$ and the engineering stress $\sigma(t)$ according to the relations $\sigma(t) = f(t)/A_c$ and $\varepsilon(t) = \Delta(t)/\ell$, where A_c is the original cross-sectional area of the sample and ℓ is the original length of the sample.

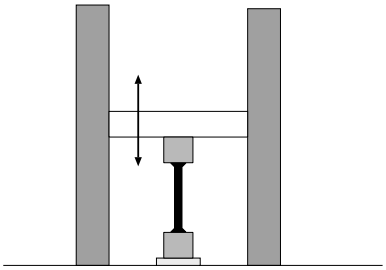

Figure 4: Quasi-static pull test on the Instron machine.

In the experiments discussed here, we used a constant strain rate of five inches per minute. At the beginning of each test, the sample was "demullinized" through a series of large displacement cycles, generally up to about 150% strain for highly-filled samples and up to 300% strain for lightly-filled samples. The Mullin's effect is a widely known phenomenon in viscoelastic materials, in which the initial load-displacement curves for a "new" sample are significantly different than those for subsequent cycles.

After the samples were demullinized, two different types of quasi-static pull tests were conducted. The first type (Type I) includes a sequence of loading and unloading the sample to produce load-displacement curves with decreasing maximum strain levels. As seen in Figure 5 with a highly-filled carbon black sample, we load and unload the rubber to create three consecutive loops at 100% maximum strain, then repeat the sequence of three loops each with maximum strain levels of 90% down to 50%. In this case, the sample is always returned to a fixed minimum strain level at the bottom of each strain loop. We used three loops of each strain level to account for and remove any possible small scale Mullin's effects.

In the second type of experiment (Type II), we created a sequence of strain loops that have decreasing maximum strain levels as before, but instead of a fixed minimum strain level we used progressively increasing minimum strain levels. As in Figure 6, we load and unload the rubber in three consecutive strain loops with a minimum strain of 25% and a maximum strain of 100%, and continue with three consecutive strain loops of 30%-90% strains, three loops of 40%-80% strains, and finally three loops of 50%-70% strains.

Using this quasi-static load and displacement data, an inverse problem can be formulated to obtain an appropriate form for our stress-strain constitutive law. Here we choose the constitutive model (3.36), and we will use parameter estimation techniques to determine the memory kernel Y and response functions g_e, g_v.

The specific forms for g_e, g_v and Y were chosen in comparison with experimental data. Based on studies detailed in [43], we chose an exponential form for the memory kernel Y. Such an exponential form generates totally nested hysteresis loops in the stress-strain curves, a feature also observed in our data (e.g., see Figures 5 and 6). For C_1 and C_2 positive, we define

$$Y(t) = C_2 e^{-C_1 t}.$$

We tried a number of linear and nonlinear functions for g_e and g_v, including the special cases of g_e and g_v linear with $g_v \equiv g_{vi} \equiv g_{vd}$. The relative errors discussed in [43] suggested that nonlinear functions are necessary for both g_e and g_v. Additional curve fitting studies outlined in [43] led to our choice of cubic polynomials for g_e, g_{vi} and g_{vd}. That is, we chose parameterized nonlinearities

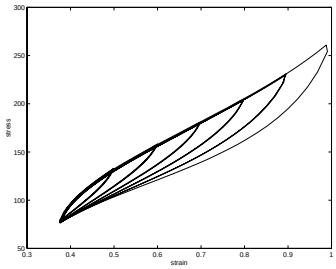

Figure 5: Quasi-static stress-strain data for highly filled carbon black: Type I.

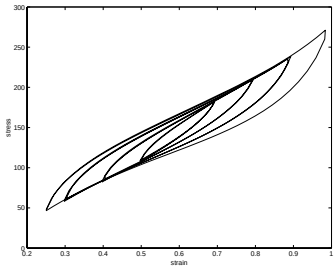

Figure 6: Quasi-static stress-strain data for highly filled carbon black: Type II.

of the form

$$g_e(x) = \sum_{i=0}^{3} E_i x^i, \qquad g_{vi}(x) = \sum_{i=0}^{3} a_i x^i, \qquad g_{vd}(x) = \sum_{i=0}^{3} b_i x^i,$$

where E_i, a_i, b_i, $i = 0, 1, 2, 3$ are real constants.

Note that the constants C_1, C_2 and E_i, a_i, b_i are material parameters, which we must determine with parameter estimation techniques. Using the experimental strain and stress data $(\hat{\varepsilon}(t_j), \hat{\sigma}(t_j))$, $j = 1, \ldots, N$ with our model (3.36), we solved for the "optimal" parameters $\vec{q} = \{C_1, C_2, E_i, a_i, b_i\}$, $i = 0, 1, 2, 3$. That is, we sought to find the parameters $\vec{q}$ that minimized

$$J(\vec{q}) = \sum_{j=1}^{N} |\hat{\sigma}(t_j) - \sigma(t_j; \vec{q})|^2 \tag{3.48}$$

over $\vec{q}$ in some admissible parameter set Q, where $\sigma(t_j; \vec{q})$ denotes the stress obtained at time t_j when inserting the strain data $\hat{\varepsilon}(t_j)$ into (3.36) with parameters $\vec{q}$.

We implemented the inverse problem on four different elastomer samples, including a silica-filled silicone material, and three natural rubber samples filled with varying levels of carbon black. Here we will present results for the silica sample (Sil), the medium-filled carbon black (CB-m) and the highly-filled carbon black (CB-h) samples.

For each elastomer, we would like our model to predict a set of nested stress-strain loops like those found in Figure 5 or 6. However, we would like to use as little data as possible in solving the inverse problem, while still obtaining accurate predictions of the full data set. After experimenting with different data sets in the inverse problem, we chose to use one or two of the stress-strain loops as the data for the inverse problem, depending on the type of data and elastomer.

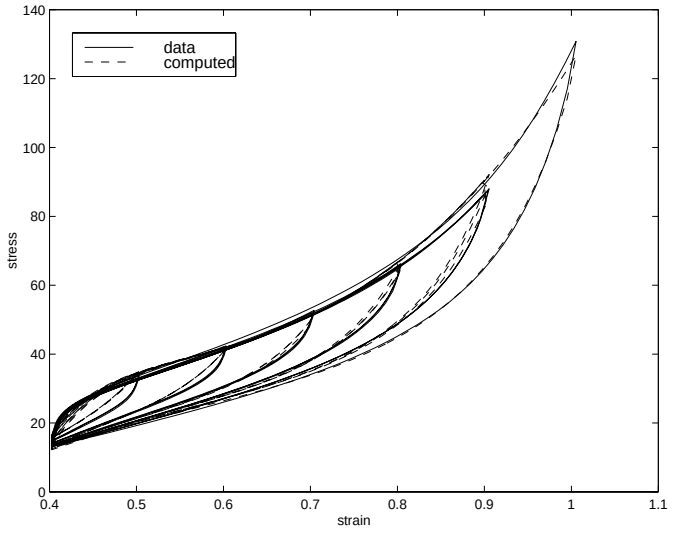

Figure 7: Type I Sil results.

For the Sil sample, we have Type I stress-strain data that was collected in the same manner as that depicted in Figure 5 for the CB-h sample. Our initial attempts at solving the inverse problem for (3.48) with this data involved using the third 100% strain loop only. We used BFGS-type optimization routines [41] to solve for the optimal parameters $\vec{q}^*$, and then used these parameters and the entire set of strain data $\hat{\varepsilon}(t_i)$ in (3.36) to predict the remaining inner loops. While these parameters could accurately match the 100% loop used in the inverse problem, they did not result in a very good prediction of the full data set. As an alternative, we chose the same 100% strain loop in addition to the first 90% strain loop to be our data in the inverse problem. The resulting parameters $\vec{q}^*$ gave substantially better predictions of the full data set, as seen in Figure 7. In this and subsequent figures, the solid lines are data plots while the dashed lines are model-computed response curves using the optimal parameters in the model. We calculated the total relative error, given by

$$\frac{\sum_{j=1}^{N} |\hat{\sigma}(t_j) - \sigma(t_j; \vec{q})|^2}{\sum_{j=1}^{N} |\hat{\sigma}(t_j)|^2},$$

and obtained a value of 3.72% for the predictions depicted in Figure 7.

The same process was repeated using Type I data from the CB-h sample. Using the third 100% strain loop and first 90% strain loop as data in the previous inverse problem, we obtained optimal parameters $\vec{q}^*$. As seen in Figure 8, these parameters yield satisfactory predictions of the whole data set, with a total relative error of 2.16%.

Next we used Type II data from the CB-h sample to solve for the optimal parameters $\vec{q}^*$. In this case we used the third 25%-100% loop as our data in solving the inverse problem, and found that the resulting parameters could successfully predict the entire data set (see Figure 9), with a total relative error of 1.36%. In a similar manner, we carried out this procedure for the CB-m Type II data and obtained parameters that could very closely predict the entire data set. The resulting prediction is seen in Figure 10, with a total relative error of 0.66%.

The parameters we obtained in each of the above inverse problems are shown in Table 1. Notice

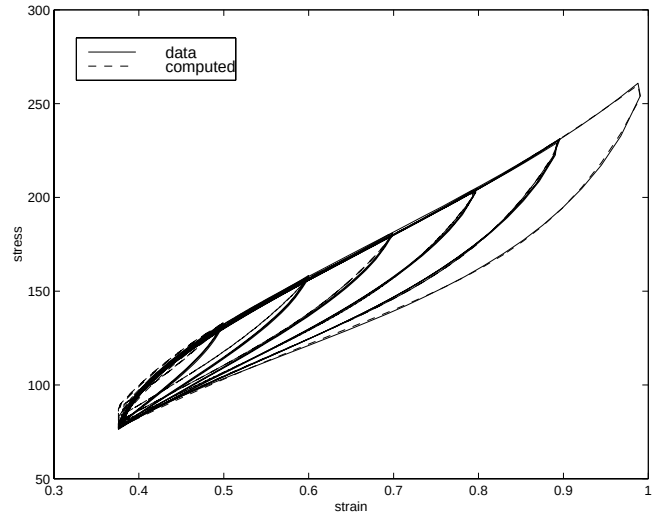

Figure 8: Type I CB-h results.

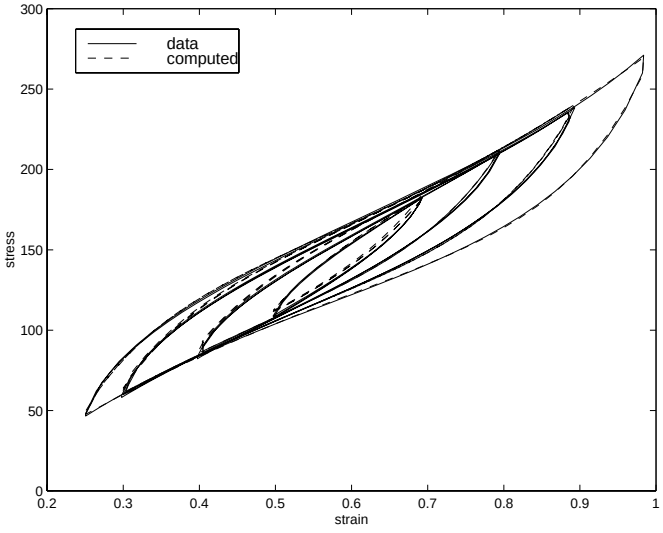

Figure 9: Type II CB-h results.

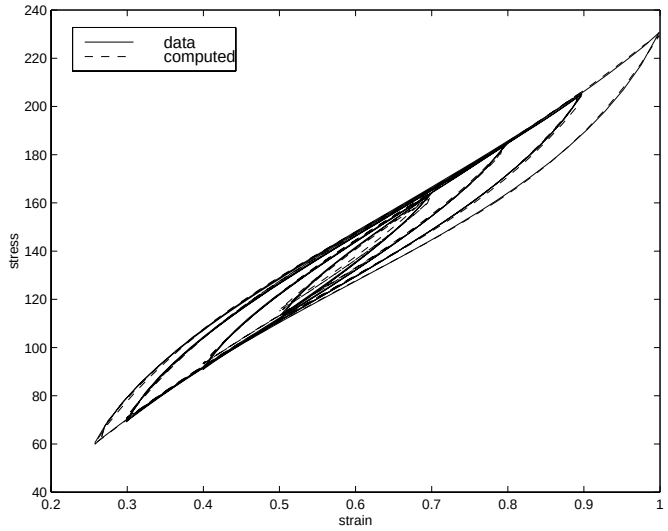

Figure 10: Type II CB-m results.

	Type I data		Type II data	
	Sil	CB-h	CB-h	CB-m
C_1	0.1836	0.2057	0.2071	0.1505
C_2	29.4541	12.9407	12.9174	7.6479
E_0	110.5593	95.2730	97.4898	63.7543
E_1	−39.7015	111.7723	113.2974	114.9653
E_2	−356.7599	−82.2648	−80.9622	−80.1991
E_3	325.0017	95.0262	96.8048	88.6977
a_0	8.6374	−0.7231	−3.1990	−7.1415
a_1	−43.9782	−14.4100	−13.6314	7.5475
a_2	46.4957	12.5035	13.3965	22.2873
a_3	1.9585	10.6746	11.2061	−2.2989
b_0	−18.2117	19.5202	19.4524	19.5571
b_1	117.3161	122.3481	122.8298	107.1207
b_2	−126.4088	−124.8175	−124.0265	−138.6131
b_3	37.9365	50.2130	50.9784	56.6247

Table 1: Optimal parameters obtained from inverse problems.

that the parameters obtained for the CB-h sample with Type I data are very similar to those found using Type II data, which suggests that these may indeed be "material" parameters. In fact, when using the parameters from the Type I CB-h inverse problem to predict the Type II CB-h data set, the total relative error was just 2.75%.

3.3.2 Dynamic inverse problems

Our hysteretic model (3.43)-(3.47) was tested on a series of dynamical experiments with different types of filled rubber samples at Lord Corporation. The primary goal of these experiments was to determine the elastic and viscoelastic response through the energy dissipation mechanism. We used the same free release experiments that were described in Section 2.2. Since the dynamical behavior of the unfilled natural rubber sample was adequately described by our basic model without hysteresis, we began our hysteresis investigations using the lightly filled sample. For given ρ, g_e, g_v and Y we solve the partial differential equation (3.43)-(3.47) forward in time, and obtain the displacement $u(t,x)$, $0 \le x \le \ell$. The data collected in these experiments provides us with the force at the top of the sample ($x = 0$), and we compare it to the force predicted by the model at the same point, given by

$$A_c\sigma(t,0) = A_c\left[g_e(u_x(t,0)) + \int_{t-r}^{t} Y(t-s)\frac{d}{ds}g_v(u_x(s,0),\dot{u}_x(s,0))ds\right],$$

where we use our computed solution $u(t,x)$ to find $u_x(t,0)$ and $\dot{u}_x(s,0)$. Our goal is to find ρ, g_e, g_v and Y so that the model predicted force at $x = 0$ best matches the data collected by the load cell. Thus, if we choose the functions $g_e(\xi) = E_1\xi + E_2\xi^2 + E_3\xi^3$, $g_{vi}(\xi) = a_1\xi + a_2\xi^2 + a_3\xi^3$, $g_{vd}(\xi) = b_1\xi + b_2\xi^2 + b_3\xi^3$, and $Y(\tau) = c_2e^{-c_1\tau}$, we can set up a parameter identification problem to find $\rho, E_1, E_2, E_3, a_1, a_2, a_3, b_1, b_2, b_3, c_1, c_2$ (collectively denoted by q) such that

$$J(q) = \sum_{i=1}^{M} |z_i - A_c\sigma(t_i, 0; q)|^2$$

is minimized. Here the z_i, $i = 1, ..., M$ are the data collected by the load cell, and $\sigma(t_i, 0; q)$ is given by the model as described above. The particular form for g_e, g_v and Y was motivated by their success in the quasi-static case. However, in our first calculations for the lightly filled rubber rod we assumed that a linear g_v, with $g_v = g_{vi} = g_{vd}$ would be sufficient to account for the slight hysteresis shown by the sample. Our time domain approximations showed good agreement with the data, but there were some discrepancies in the frequency domain comparisons. Thus we proceeded to assume that g_v was a cubic polynomial with $g_v(\xi) = g_{vi}(\xi) = g_{vd}(\xi) = a_1\xi + a_2\xi^2 + a_3\xi^3$. We also chose the Kelvin-Voigt damping coefficient $C_D = 0$. This damping term is important for the theoretical result but in our experiments and computations we have determined that the hysteresis portion of the model can provide adequate damping to capture the dynamic behavior. In our computations we used linear splines for spatial discretization, i.e., we were looking for the displacement $u(t,x) = \sum_{i=1}^{N} u_i(t)\phi_i(x)$, where ϕ_i are the usual piecewise linear splines:

$$\phi_i(x) = \begin{cases} \frac{1}{h}x - (i-1) & (i-1)h \le x \le ih \\ -\frac{1}{h}x + (i+1) & ih \le x \le (i+1)h \\ 0 & otherwise. \end{cases} \tag{3.49}$$

In solving the system (3.43)-(3.47) forward in time, the treatment of the hysteresis integral proved to be very time consuming. Since this computation needs to be repeated for each set of parameters

during the optimization, the computational parameter identification process was very time consuming. Hence, we formulated an equivalent system to (3.43)-(3.47) using internal variables and used it in the above framework for our subsequent calculations. This system is given by

$$\rho A_c \ddot{u} - \frac{\partial}{\partial x}\left(A_c g_e(u_x) + A_c \epsilon_1\right) = F(t) \quad \text{in } V^* \tag{3.50}$$

$$\dot{\epsilon}_1 = -c_1 \epsilon_1 + \frac{d}{dt}(g_v(u_x, \dot{u}_x)) \tag{3.51}$$

$$u(t,0) = 0 \tag{3.52}$$

$$u(0,x) = 0 \tag{3.53}$$

$$u_t(0,x) = 0 \tag{3.54}$$

$$\epsilon_1(0,x) = 0, \tag{3.55}$$

where, in general, the derivatives of g_v in (3.51) are distributional. For the special case $g_v = g_{vi} = g_{vd}$, of course, ordinary derivatives suffice.

The parameter identification problem was solved using MATLAB optimization routines. As we described earlier, the free release experiments for the lightly filled sample were repeated with different amounts of tip mass, namely 3 lb, 2 lb and 1 lb. Our results for the identification problem are shown in Figures 11-13. The parameters that we found in the different cases are presented in Table 2.

As depicted in Figure 14, the resulting elastic response functions g_e differ slightly in the experiments with different amounts of tip mass. It is worth noting that the same elastic response was identified in each case even when we took g_v to be linear in our first calculations.

By averaging the g_e's that we found, we used a 'universal' elastic response in the different cases and solved the parameter identification problem for g_v and c_1. This did not prove to be successful, since we could not get closer to the data than 10% relative error in the case of the experiments with 1 and 3 lb extra weight, whose g_e was further away from the 'average'. One possible explanation for this behavior *may be* that the elastic response itself should also be strain-rate dependent. Our current model does not take this into account. We also remark that there is substantial difference in the maximum dynamic strain achieved during these experiments see Table 3. Thus, not only does the average strain rate very from one experiment to the other, but also the ranges of the strain amplitudes differ substantially.

We plotted the identified viscoelastic nonlinearity in each case in Figure 15. These functions show remarkable agreement. Although they are almost linear, they perform noticeably better in the frequency domain than a linear approximation for g_v.

However, not surprisingly, one finds that c_1 and g_v are not unique solutions to the least squares minimization in the sense that comparable fits can be achieved in both the time and frequency domain using very different parameters for c_1 and g_v. For example, Figures 16-17 depict two fits, one with the previously identified c_1 and g_v from Table 2, and one with $g_v(\xi) = e^{4.15}\xi - 22.77\xi^2 + 4.23\xi^3$, $c_1 = e^{3.71}$ for the 3 lb extra weight and respectively, for the 2 lb extra weight, with the previous c_1 and g_v and with $g_v = e^{4.04}\xi - 23.63\xi^2 + 4.07\xi^3$, $c_1 = e^{4.06}$. This suggests that it may not be possible to identify these parameters individually with only this data for the sample.

Current efforts in our numerical investigations involve the highly filled rubber sample. Since in this case the hysteretic effect is very pronounced, we cannot expect to obtain adequate results with

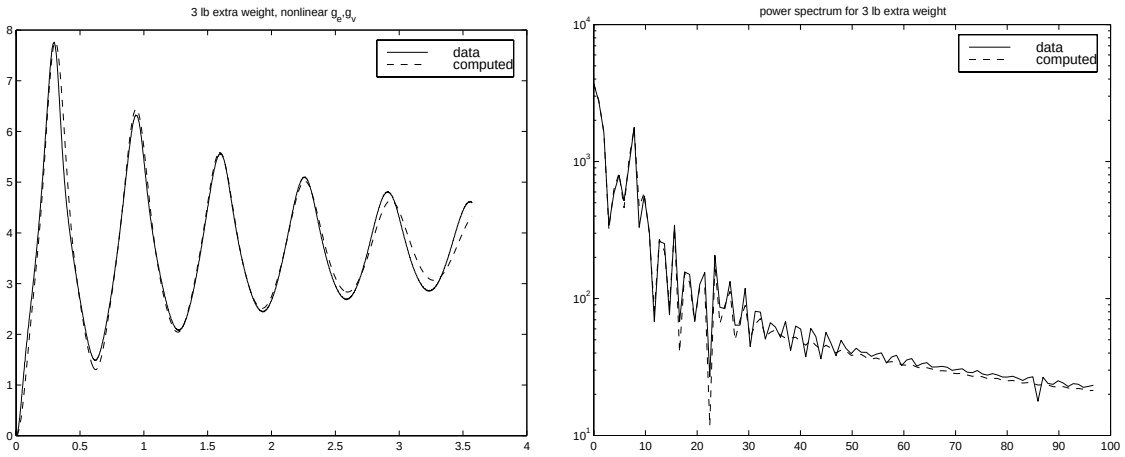

Figure 11: (left) Time domain approximation with a nonlinear g_e, g_v, 3 lb extra weight, 4.4% relative error, and (right) the power spectrum of the solution and the data.

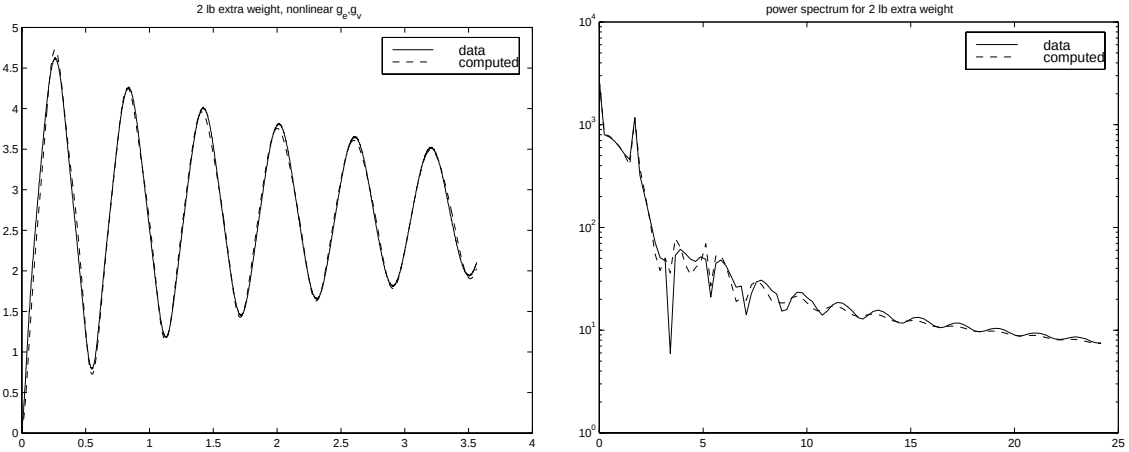

Figure 12: (left) Time domain approximation with a nonlinear g_e, g_v, 2 lb extra weight, 3% relative error, and (right) the power spectrum of the solution and the data.

		3 lb	*2 lb*	*1 lb*
	ρ	0.00010	0.00011	0.00011
	c_1	$e^{8.37}$	$e^{8.75}$	$e^{8.8325}$
g_e	E_1	112.88	141.51	191.33
	E_2	-39.74	-64.645	-167.6165
	E_3	8.69	15.311	71.6774
g_v	a_1	$e^{7.54}$	$e^{7.47}$	$e^{7.51}$
	a_2	-108.67	-107.14	-102.92
	a_3	106.01	109.97	118.39

Table 2: Identified parameters for the dynamic experiments with the lightly filled sample

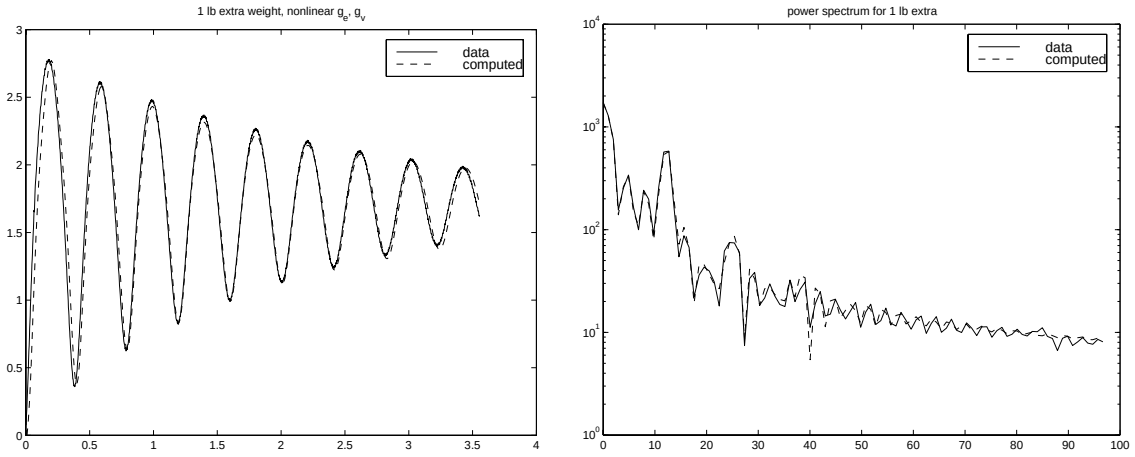

Figure 13: (left) Time domain approximation with a nonlinear g_e, g_v, 1 lb extra weight, 4.1% relative error, and (right) the power spectrum of the solution and the data.

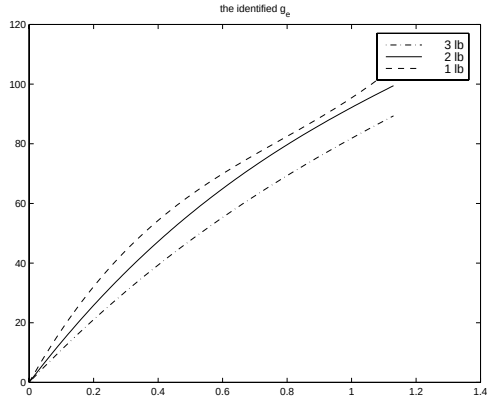

Figure 14: The identified g_e

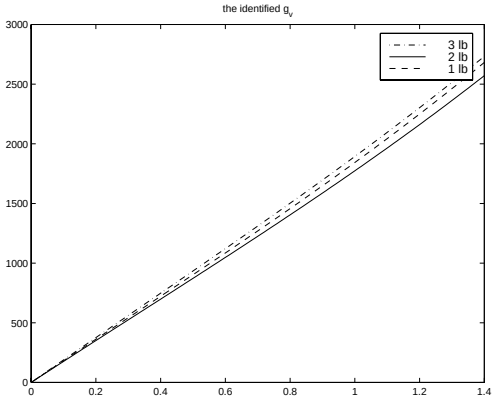

Figure 15: The identified g_v

weight	*strain range*
3 lb	330% - 230%
2 lb	240% - 150%
1 lb	120% - 70%

Table 3: Strain ranges obtained in dynamic experiments.

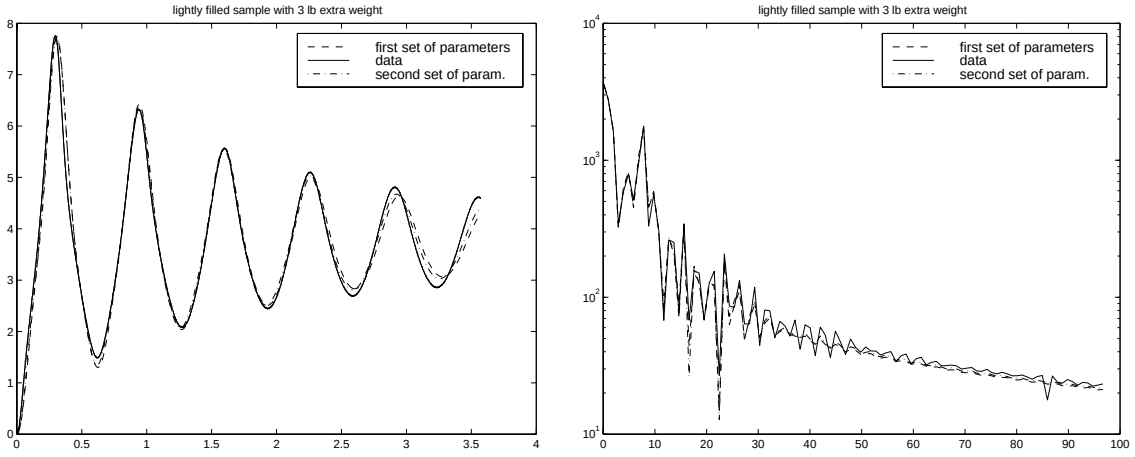

Figure 16: (left) Time domain approximation with two different g_v's for 3 lb extra weight, and (right) the same approximation in the frequency domain.

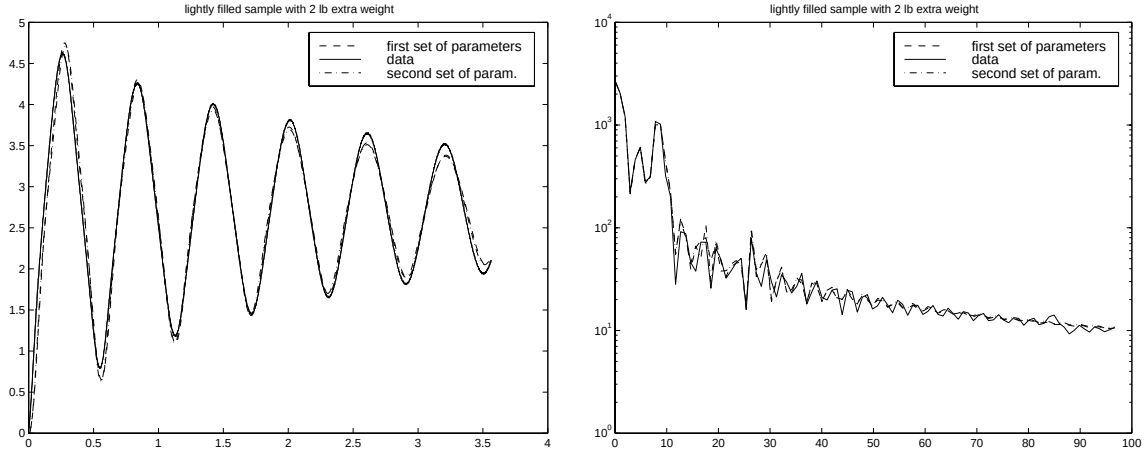

Figure 17: (left) Time domain approximation with two different g_v's for 2 lb extra weight, and (right) the same approximation in the frequency domain.

$g_v(\xi) = g_{vi}(\xi) = g_{vd}(\xi)$. That is, we have to account for the different loading and unloading paths in the viscoelastic response. Thus for the highly filled rubber sample we are using

$$g_v(\varepsilon(s), \dot{\varepsilon}(s)) \quad = \quad \begin{cases} g_{vi}(\varepsilon(s)) = \sum_{i=0}^{3} a_i \varepsilon^i(s) & \dot{\varepsilon}(s) > 0 \\ g_{vd}(\varepsilon(s)) = \sum_{i=0}^{3} b_i \varepsilon^i(s) & \dot{\varepsilon}(s) < 0, \end{cases} \tag{3.56}$$

in solving the full model. This work is currently in progress, but initial results are most encouraging.

4 Concluding Remarks

In the above presentation we have outlined our progress to date in the development of nonlinear hysteretic dynamic models for MR based elastomers. Substantial experimental validation for our approach is provided in the quasi-static case. Significant efforts are still required to achieve similar status in the full dynamic case. Modeling of samples in shear is underway and represents an important component of our overall investigations. Moreover, to attain the level of modeling required for design and feedback control of active MR elastomers, a major effort remains on response of the elastomer in the presence of an external magnetic field.

5 Acknowledgments

We are grateful to Yue Zhang (current address: Michelin North America) and N.J. Lybeck (current address: Applied Math, Inc.) for their substantial contributions to some of the earlier efforts described above.

We would also like to thank Richard Wilder of Lord Corporation for his help with implementing the experiments.

This research was supported in part by the U.S. Air Force Office of Scientific Research under grants AFOSR F49620-95-1-0236, AFOSR F49620-95-1-0375, AFOSR F49620-98-1-0180, and in part by an NSF-GRT fellowship to L.K.P. under grant GER-9454175.

References

[1] H.T. Banks, R.H. Fabiano and Y. Wang, "Estimation of Boltzmann damping coefficients in beam models", *Proceedings of COMCON Workshop on Stabilization of Flexible Structures*, A.V. Balakrishnan and J.P. Zolesio, eds., Optimization Software Inc., New York, (1987), 13-35.

[2] H.T. Banks, R.H. Fabiano and Y. Wang, "Inverse problem techniques for beams with tip body and time hysteresis damping", *Mat. Aplic. e Comput.* **8** (1989), 101-118.

[3] H.T. Banks, R. Fabiano, Y. Wang, D. Inman and H. Cudney, "Spatial versus time hysteresis in damping mechanics", *Proc. 27th IEEE Conf. on Dec. and Control* (1988), 1674-1677.

[4] H.T. Banks, D.S. Gilliam and V.I. Shubov, "Global solvability for damped abstract nonlinear hyperbolic systems", *Differential and Integral Equations* **10** (1997), 309-332.

[5] H.T. Banks and N. Lybeck, "Modeling methodology for elastomer dynamics", in *Systems and Control in the 21st Century*, Birkhäuser, Boston, 1996, 37-50.

[6] H.T. Banks, N.J. Lybeck, M.J. Gaitens, B.C. Muñoz and L.C. Yanyo, "Computational methods for estimation in the modeling of nonlinear elastomers", CRSC-TR95-40, NCSU; *Kybernetika* **32** (1996), 526-542.

[7] H.T. Banks, N.G. Medhin, and Y. Zhang, "A mathematical framework for curved active constrained layer structures: well-posedness and approximation", CRSC-TR95-32, NCSU; *Numerical Functional Analysis & Optimization* **17** (1996), 1-22.

[8] H.T. Banks and G.A. Pinter, "Approximation results for parameter estimation in nonlinear elastomers", CRSC-TR96-34, NCSU; *Control and Estimation of Distributed Parameter Systems*, F. Kappel, et.al.,eds., Birkhäuser, Boston, 1997.

[9] H.T. Banks, G.A. Pintér, and L.K. Potter, "Existence of unique weak solutions to a dynamical system for nonlinear elastomers with hysteresis," CRSC-TR98-43, NCSU, Nov. 1998; *Differential and Integral Equations,* to appear.

[10] H.T. Banks, L.K. Potter and Y. Zhang, "Stress-strain laws for carbon black and silicon filled elastomers", *Proc. 36th IEEE Conf. on Dec. and Control* (1996), 3727-3732.

[11] H.T. Banks, R.C. Smith and Y. Wang, *Smart Material Structures: Modeling, Estimation and Control*, Masson, Paris and John Wiley and Sons, Chichester, 1996.

[12] A. Bensoussan, J.L. Lions and G. Papanicolaou, *Asymptotic Analysis for Periodic Structures*, North-Holland, New York, 1978.

[13] R. Bloch, W.V. Chang and N.W. Tschoegl, "The behavior of rubberlike materials in moderately large deformations", *Journal of Rheology* **22** (1978), 1-32.

[14] R. Bloch, W.V. Chang and N.W. Tschoegl, "On the theory of the viscoelastic behavior of soft polymers in moderately large deformations", *Rheologia Acta* **15** (1976), 367-378.

[15] D.J. Charlton, J. Yang, and K.K. Teh, "Mechanical properties of solid polymers," *Rubber Chemistry & Technology* **67** (1994), 481-503.

[16] R.M. Christensen, *Theory of Viscoelasticity: An Introduction*, 2nd ed., Academic Press, New York, 1982.

[17] M. Codegone and A. Negro, "Homogenization of the nonlinear quasistationary Maxwell equations with degenerated coefficients", *Applicable Analysis* **18** (1984), 159-173.

[18] A. Defranceschi, "An Introduction to Homogenization and G-Convergence", *Lecture Notes, School on Homogenization, ICTP, Trieste, Sept.6-8, 1993.*

[19] M. Doi and M. Edwards, *The Theory of Polymer Dynamics*, Oxford, New York, 1986.

[20] W.N. Findley, J.S. Lai and K. Onaran, *Creep and Relaxation of Nonlinear Viscoelastic Materials*, H.A. Lauwerier and W.T. Koiter, eds., North-Holland Series in Applied Mathematics and Mechanics, North-Holland Publishing Company, 1976.

[21] J.D. Ferry, *Viscoelastic Properties of Polymers*, John Wiley & Sons, Inc., New York, 1980.

[22] M.I. Friswall, D.J. Inman and M.J. Lam, "On the realisation of GHM models in viscoelasticity", preprint, 1997.

[23] M.V. Gandhi and B.S. Thompson, *Smart Materials and Structures*, Chapman and Hall, London, 1992.

[24] D.F. Golla and P.C. Hughes, "Dynamics of viscoelastic structures — A time-domain, finite element formulation", *ASME J. Applied Mechanics* **52** (1985), 897-905.

[25] V.V. Jikov, S.M. Kozlov and O.A. Oleinik, *Homogenization of Differential Operators and Integral Functionals*, Springer Verlag, New York, 1994.

[26] A.R. Johnson, C.J. Quigley and J.L. Mead, "Large strain viscoelastic constitutive models for rubber, part I: Formulations", *Rubber Chemistry Technology* **67** (1994), 904-917.

[27] A.R. Johnson, A. Tessler and M. Dambach, "Dynamics of thick elastic beams", *J. Engr. Materials and Tech.* **119** (1997), 278-278.

[28] A.R. Johnson and R.G. Stacer, "Rubber viscoelasticity using the physically constrained systems' stretches as internal variables", *Rubber Chem. Tech.* **66** (1993), 567-577.

[29] M.R. Jolly, J.D. Carlson and B.C. Muñoz, "A model of the behavior of magnetorheological materials", *Smart Mater. Struct.* **5** (1996), 607-614.

[30] M.R. Jolly, J.D. Carlson, B.C. Muñoz and T.A. Bullions, "The magnetoviscoelastic response of elastomer composites consisting of ferrous particles embedded in a polymer matrix", *Journal of Intelligent Material Systems and Structures* **7** (1996), 613-622.

[31] H. Kolsky, "The measurement of the material damping of high polymers over ten decades of frequency and its interpretation", V. K. Kinra and A. Wolfenden, eds., *Mechanics and Mechanisms of Material Damping*, American Society for Testing and Materials, Philadelphia, 1992.

[32] G.A. Lesieutre, "Modeling frequency-dependent longitudinal dynamic behavior of linear viscoelastic long fiber components," *J. Composite Materials* **28** (1994), 1770-1782.

[33] G.A. Lesieutre and K. Govindswamy, "Finite element modeling of frequency-dependent and temperature-dependent dynamic behavior of viscoelastic materials in simple shear," *Int. J. Solids Structures* **33** (1996), 419-432.

[34] D.J. McTavish, P.C. Hughes, Y. Soucy and W.B. Graham, "Prediction and measurement of modal damping factors for viscoelastic space structures", *AIAA Journal* **30** (1992), 1392-1399.

[35] B.C. Muñoz and M.R. Jolly, "Composites with field responsive rheology", W.K. Brostow, ed., *Performance of Plastics*, Hansen Publishers, N.Y., 1997.

[36] R.W. Ogden, *Non-linear Elastic Deformations*, Ellis Horwood Limited, Chichester, 1984.

[37] A. Rivera-Dominguez and W.M. Jordan, "Predictive creep response of linear viscoelastic graphite/epoxy composites using the Laplace Transform method", *Journal of Materials Engineering and Performance* **1** (1992), 261-266.

[38] R.S. Rivlin, "Large elastic deformations of isotropic materials, I, II, III." *Phil. Trans. Roy. Soc. A* **240** (1948), 459-525.

[39] R.A. Schapery, "On the characterization of nonlinear viscoelastic materials", *Polymer Engineering and Science* **9** (1969), 295-310.

[40] T.M. Simon, F. Reitich, M.R. Jolly, K. Ito and H.T. Banks, "Estimation of the effective permeability in magnetorheological fluids, CRSC-TR98-35, NCSU, Oct. 1998; *J. Intelligent Mat. Systems and Structures*, submitted.

[41] J. Stoer and R. Bulirsch, *Introduction to Numerical Analysis,* Springer-Verlag, New York, 3rd ed. (1993).

[42] I.M. Ward, *Mechanical Properties of Solid Polymers,* John Wiley & Sons, New York, 2nd ed. (1983).

[43] Y. Zhang, *Mathematical formulation of vibrations of a composite curved beam structure: Aluminum core material with viscoelastic layers, constraining layers and piezoceramic patches*, Ph.D. Thesis, N.C. State University, May 1997.